A Triangle Based Finite Volume Method for the Integration of Lubrication's Incompressible Bulk Flow Equations

Mihai Arghir
e-mail: mihai.arghir@lms.univ-poitiers.fr

Jean Frêne
e-mail: jean.frene@lms.univ-poitiers.fr

LMS, Université de Poitiers,
URF Sciences SP2MI, Téléport 2,
Blvd. Pierre et Marie Curie, BP 30719,
86962 Futuroscope Chasseneuil Cedex,
France

It is well known that for a reduced Reynolds number ($Re^* = \rho VH/\mu \cdot H/L$) greater than unity, inertia forces have a dominant effect in the transport equations, thus rendering the classical lubrication equation inapplicable. The so called "bulk flow" system of equations is then the appropriate mathematical model for describing the flow in bearing and seals operating at $Re^* \geqslant 1$. The difficulty in integrating this system of equations is that one has to deal with coupled pressure and velocity fields. Analytic methods have a very narrow application range so a numerical method has been proposed by Launder and Leschziner in 1978. It represents a natural extrapolation of the successful SIMPLE algorithm applied to the bulk flow system of equations. The algorithm used rectangular, staggered control volumes and represented the state of the art at that moment. In the present work we introduced a method using triangular control volumes. The basic advantage of triangles versus rectangles is that non rectangular domains can be dealt without any a priori limitation. The present paper is focused on the description of the discretized equations and of the solution algorithm. Validations for bearings and seals operating in incompressible, laminar and turbulent flow regime are finally proving the accuracy of the method. [DOI: 10.1115/1.1326444]

Introduction

Usual incompressible lubrication flows are characterized by zero or negligible convective inertia effects. The first result of the two length scale dimensional analysis performed on the flow motion governing equations is that convective inertia terms have the order of magnitude of the reduced Reynolds number

$$\mathrm{Re}^* = \mathrm{Re}\frac{H}{L} \quad \left(\mathrm{Re} = \frac{\rho VH}{\mu}\right), \tag{1}$$

where H and L are the characteristic length scales, the former being based on the film thickness and the second on the film length. For usual systems H/L is of the order of 10^{-3} or less and the Reynolds number is not large enough, so $\mathrm{Re}^* \ll 1$. Most of classical Lubrication's applications satisfy this limit but recent high power density machinery show a need of lubrication or sealing devices operating far beyond the limit of $\mathrm{Re}^* = 1$. The inclusion of inertia forces in the flow governing equations is then a must and obtaining a solution is a more difficult task due to their nonlinear character. An overview of the problem was given by Constantinescu [1].

The first solutions of the complete system of equations used small perturbation approaches applied to the boundary layer type of flow equations [2,3]. Their application to general cases being difficult, development activities became focused on full numerical solutions. First, the equations were adapted to flows between two closely spaced walls by making a film thickness average of flow variables. This approach, which borrows something from the derivation of the classical Reynolds lubrication equation, was first due to Slezkin and Targ [4] and was subsequently used by Constantinescu some three decades ago to deduce the system of equation of visco-inertial flow in thin layers. His approach was to start from the boundary layer type of equations, to suppose a laminar like velocity profile unmodified by inertia forces injected in these equations and then to make a film thickness average. An apparently different approach for obtaining the same set of equations evolved during the last two decades and its presentation can be found in the work of Childs [5]. Following this derivation, the flow governing equations are obtained by writing a conservation balance for an infinitesimal control volume extending from the upper to the lower wall, all flow variables being considered constant across the film thickness. Known as the bulk flow system of equations, this set is not different from the previous one. By taking into account the velocity profile, Constantinescu obtained some correction terms in the equations but without changing their nature. It is difficult to appreciate which set of equations is better. For laminar flow, it is clear that taking into account the form of the velocity profile is rigorously correct but for turbulent flow the approach can be questioned. The velocity profile in turbulent flow is very blunt, almost constant if one discards the very rapid variation close to the walls, so directly considering an averaged value would be a good hypothesis. This and the fact that most inertia dominated flows are also highly turbulent lead to a widespread use of the bulk flow equations.

The best general solution was given by Launder and Leschziner [6]. They dealt with the form of the equations given by Constantinescu and they observed that a powerful numerical tool, the SIMPLE algorithm, developed in the seventies for the complete Navier-Stokes equations (for which a presentation is given in [7]), could also be applied to inertia dominated lubrication flows. The numerical solution they proposed used a rectangular grid and in order to ensure the coupling of velocity and pressure fields, staggered control volumes were used for each of the flow variables. Stability was preserved by using a first order upwind approach for the convective derivatives although more accurate approaches became lately available. Under this form the algorithm represented the state of the art at that moment and was successfully used by San Andrès and coworkers in numerous high Reynolds number applications. The main drawback of this numerical solution is its lack of flexibility. Rectangular control volumes can deal only with

Contributed by the Tribology Division for publication in the ASME JOURNAL OF TRIBOLOGY. Manuscript received by the Tribology Division March 6, 2000; revised manuscript received July 25, 2000. Associate Editor: J. L. Streator.

regular geometries because the interior boundaries of the discretization must coincide with the discontinuities of the analysis domain. The analysis of bearings or seals with arbitrarily shaped pockets and grooves is then excluded.

Substantial progress have been made in the field of numerical analysis since Launder and Leschziner proposed their solution two decades ago. Unstructured grids became widely used not only for elasticity problems but for convection dominated flows also. Finite element solution of the transport equations started to compete finite volume ones [8,9]. The main cause that delayed the introduction of unstructured grids in conjunction with the finite volume SIMPLE algorithm was the necessity to stagger the velocity control volumes in its first formulation. Solutions to overcome this problem were given by Rhie and Chow [10] and by Peric [11]. Once this problem passed by, SIMPLE based solutions for the Navier-Stokes equations on unstructured grids were proposed by Mathur and Murthy [12] and Lai [13]. The goal of the present work is the development of such of a triangular based numerical procedure for the solution of Lubrication's ''bulk flow'' incompressible and isothermal system of equations. It is the first step towards the analysis of arbitrarily shaped bearing and seals that cannot be tackled with rectangular control volumes.

Governing Equations

The system of bulk flow equations for incompressible, isothermal flow can be written under the form of three convective transport equations.

$$\mathrm{div}(\rho \vec{V} H \Xi) = S_{\Xi} \tag{2}$$

The source terms are presented in Table 1. The viscous part lumped in the source terms is expressed under the form proposed by Hirs [14].

$$\tau_S = \frac{1}{2}\rho f_S V_S^2, \quad \tau_R = \frac{1}{2}\rho f_R V_R^2 \tag{3}$$

$$V_S = \sqrt{W^2 + U^2}, \quad V_R = \sqrt{W^2 + (U - R\omega)^2}, \tag{4}$$

where friction factors can be expressed by Blasius' law for a laminar flow or by one of the several laws that exist for turbulent regime (Blasius, Moody, Colebrooke, etc.)

In the following, the circumferential direction $R\theta$ will be assigned by x (so $R\partial\theta = \partial x$) and will be associated with any relative velocity such as $R\omega$.

Boundary Conditions. Three types of boundary conditions, namely pressure, symmetry and periodicity, are sufficient for describing any incompressible, isothermal Lubrication problem. In the most general form, the stagnation pressure and the concentrated inertia coefficients are given on a pressure boundary

$$P^0 = P + (1 \pm \xi)\frac{\rho V_n^2}{2}, \tag{5}$$

where the plus sign holds for an inlet boundary (pressure drop effect) and the minus sign for an exit one (pressure recovery effect).

Table 1 Source terms of the incompressible and isothermal bulk flow equations

Ξ	S_{Ξ}
1	0 (continuity equation)
W	$-H\dfrac{\partial P}{\partial z} + \tau_{Sz} + \tau_{Rz} \quad (\tau_{Sz} = \tau_S \dfrac{W}{V_S},\ \tau_{S\theta} = \tau_S \dfrac{U}{V_S})$
U	$-H\dfrac{\partial P}{R\partial\theta} + \tau_{S\theta} + \tau_{R\theta} \quad (\tau_{Rz} = \tau_R \dfrac{W}{V_R},\ \tau_{R\theta} = \tau_R \dfrac{U - R\omega}{V_R})$

Symmetry boundary conditions imply $V_n = 0$ and $\partial\Xi/\partial n = 0$ for any other variable.

Numerical Solution

The solution domain for Lubrication problems can be either a rectangle (if one deals with two dimensional pads or with the developed surface of cylindrical bearings and annular seals) or a circular sector (for thrust bearings and face seals). The list could also include conical or spherical bearings but, in any case, a generalized rectangle would be an enough accurate representation.

The domain is discretized using unstructured triangular grids. The control volumes (or cells) are considered to coincide with the triangles of the discretization. So each cell has three edges and three vertices that coincide with the nodes of the mesh. Internal edges have two cells on either side while boundary edges have only one. Figure 1 presents an internal discretization cell with its three neighbors and Fig. 2 presents two different grids.

One must distinguish internal edges from boundary edges, the later having the important role of carrying boundary conditions. Edges carrying pressure or symmetry boundary conditions are grouped in the boundary edges category while periodicity edges are treated as internal ones.

All transport variables are defined at triangle's center. When needed, variables are also defined on edges at characteristic points. For internal edges, these points represent the intersection of the segment joining two adjacent cell centers with the corresponding edge (Fig. 1). For boundary edges, characteristic points lye at edge's midpoint.

Discretization of the General Transport Equation. The general transport equation is integrated on the triangular control volume.

$$\int_{\vartheta} \mathrm{div}(\rho \vec{V} H \Xi)\, d\vartheta = \int_{\vartheta} S_{\Xi}\, d\vartheta \tag{6}$$

Using the Gauss-Ostrogradski theorem for the left hand side and the midpoint rule for the right hand side yields

$$\int_{\Gamma} \rho \vec{V} H \Xi \cdot \vec{n}\, d\gamma = \sum_i \dot{m}_i \Xi_i = S_{\Xi}\vartheta, \tag{7}$$

where $\dot{m}_i = \rho V_{ni} H_i \gamma_i$ is the mass flow rate across the edge, positive if the flow leaves the control volume. The transported variable is interpolated at the characteristic point of the edge by taking

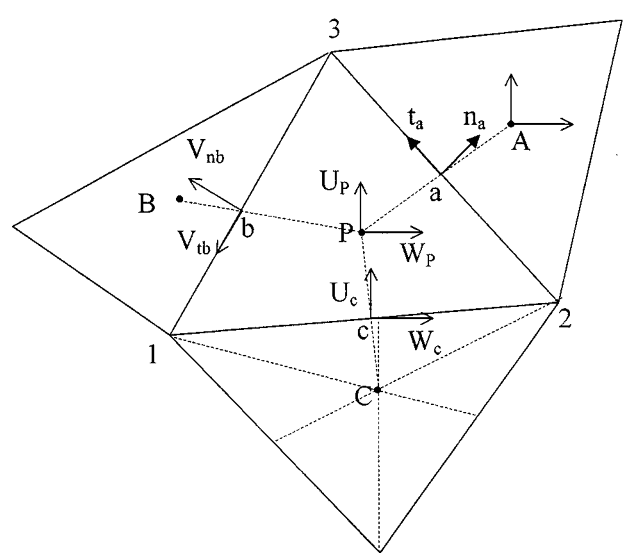

Fig. 1 Triangular control volume and its neighbors

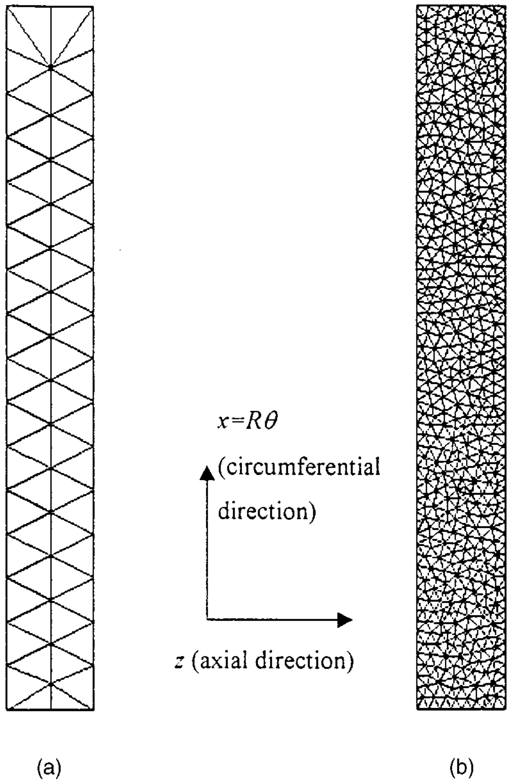

Fig. 2 Triangular grids employed (*a*) for a one-dimensional pad and (*b*) for the developed surface of circular bearings and annular seals

into account the direction of the normal velocity. The first order precision is obtained by taking the value from the ''upwind'' triangle.[1]

$$\Xi_i^{1OP}=\Xi_i^{\text{upwind}}=\Xi_P\frac{\text{SIGN}(1,V_{ni})+1}{2}-\Xi_I\frac{\text{SIGN}(1,V_{ni})-1}{2} \tag{8}$$

The higher order approximation can be considered in many ways. The most simple way is to consider the interpolated value obtained from edge's two adjacent cells [15].

$$\Xi_i^{HOP}=\Xi_P\frac{d_{Ii}}{d_{PI}}+\Xi_{Ii}\frac{d_{Pi}}{d_{PI}} \tag{9}$$

A better approach in terms of numerical stability is the upwind interpolated edge value [12].

$$\Xi_i^{HOP}=\Xi_{\substack{\text{upwind}\\ \text{cell}}}+(\text{grad}\,\Xi)_{\substack{\text{upwind}\\ \text{cell}}}\cdot\vec{d}_{Pi}\,, \tag{10}$$

where $(\text{grad}\,\Xi)_{\substack{\text{upwind}\\ \text{cell}}}$ is the reconstruction gradient at the upwind cell and $\vec{d}_{Pi}$ is the vector directed from the center of the upwind cell to the characteristic point of the edge. Ensuring stability necessitates the use of the flux limiter proposed by Venkatakrishnan [16] for the estimation of the reconstruction gradient.

Including an under-relaxation factor the discretized transport equation yields

$$a_P(1+r_\Xi)\Xi_P=\sum_{I=A,B,C}a_I\Xi_I+(S_\Xi)_P\vartheta_P+a_Pr_\Xi\Xi_P$$
$$+b_\Xi\sum_{i=a,b,c}\dot{m}_i(\Xi_i^{1OP}-\Xi_i^{HOP}) \tag{11}$$

[1]SIGN$(a,b)=a*\text{sign}(b)$ is the standard Fortran function

$$a_I=\dot{m}_i\frac{\text{SIGN}(1,V_{ni})-1}{2},\quad a_P=\sum_{I=A,B,C}a_I\,, \tag{12}$$

where the high order precision of the edge value is included explicitly using a blending factor. First order solutions obtained with $b_\Xi=0$ are very stable in terms of convergence while a blending factor $b_\Xi=1$ means that the final converged solution will have a high order precision. Values between 0 and 1 of the blending factor are used when high order precision solution are difficult to obtain, generally with coarse grids.

Boundary conditions are readily implemented and need no special treatment. A pressure boundary edge can work either as an inlet ($V_{ni}<0$) or as an exit ($V_{ni}>0$). For an inlet edge, the transported variable Ξ is either imposed as a boundary condition (namely the tangential component of the velocity vector or any scalar variable) or calculated from a mass balance equation (the normal component of the velocity vector). For an exit edge, the coefficient a_i is zero and the transported variable is extrapolated from the interior domain to the edge. For a symmetry boundary edge $V_{ni}=0$ so m_i and a_I are zero and the transported variable is calculated from a zero gradient extrapolation.

Finally, all coefficients are kept constant being known from a previous level and the linear system is iteratively solved using a Gauss-Seidel relaxation procedure up to a reasonable reduction of the initial error.

Discretization of the Continuity Equation. The discrete continuity equation is written as

$$\int_\Gamma \rho\vec{V}H\cdot\vec{n}\,d\gamma=\sum_i \dot{m}_i\,. \tag{13}$$

It is known that when velocity components and pressure are stored at cells centers, computing the face velocity V_{ni} by simply interpolating between the two adjacent cell values is prone to checkerboard instability [15]. A special momentum interpolation scheme introduced by Rhie and Chow [10] is used to avoid this.

$$V_{ni}^*=\overline{V_{ni}^*}-\overline{\left[\frac{H_P\vartheta_P}{a_P(1+r_V)}\right]}_i\left[\left(\frac{\partial P}{\partial n}\right)_i-\overline{\left(\frac{\partial P}{\partial n}\right)}_i\right]$$
$$+\frac{r_V}{1+r_V}[V_{ni}-\overline{(\vec{V})}_i\cdot\vec{n}_i] \tag{14}$$

where W^* and U^* are velocity components obtained after solving the discrete transport equations and $\overline{\text{« »}}$ are edge interpolated values. The same underrelaxation coefficient r_V is used for W and U transport equations. The values in the last term are estimated from a previous iteration level and are introduced in order to avoid an underrelaxation factor dependence of the converged solution [17].

The central point of the SIMPLE algorithm is the coupling between the velocity and the pressure field. It is supposed that these variables can be written as a prediction plus a correction value.

$$W=W^*+W',\quad U=U^*+U',\quad P=P^*+P' \tag{15}$$

The prediction values for velocities are obtained from solving the momentum equations while the first value for the pressure is estimated from an informed guess. Corrections are calculated by enforcing the continuity equations as in the following.

By using the decomposed field values, the mass flux and the discrete continuity equation can be written as follows:

$$\sum_i(\dot{m}_i^*+\dot{m}_i')=0 \tag{16}$$

$$\dot{m}_i^*=\rho V_{ni}^*H_i\gamma_i\,,\quad \dot{m}_i'=\rho V_{ni}'H_i\gamma_i\,. \tag{17}$$

It is supposed that the correction of the normal velocity depends only on the corrected pressure gradient yielding

$$V'_{ni} = -\overline{B}_i \left(\frac{\partial P'}{\partial n}\right)_i \approx -\overline{B}_i \left(\frac{\partial P'}{\partial \zeta}\right)_i = -\overline{B}_i \frac{P'_I - P'_P}{d_{PI}}. \quad (18)$$

In the above estimation of the pressure gradient it was assumed that directions $\vec{n}$ and $\vec{\zeta}$ are very close. The assumption is well verified for a Delauney triangulation and can be further sustained by observing that the accepted error is of the order of $(\text{grad}\, P')_i \cdot (\vec{n} - \vec{\zeta})_i$ and tends to zero for a converged solution [15].

Finally, the discrete continuity equation yields a linear system for pressure corrections.

$$a_P P'_P = \sum_{I=A,B,C} a_I P'_I - \sum_{i=a,b,c} \dot{m}_i^* \quad (19)$$

$$a_I = \frac{\rho B_i H_i \gamma_i}{d_{PI}}, \quad a_P = \sum_{Ii=A,B,C} a_I \quad (20)$$

On a pressure boundary edge, P' is zero. On a symmetry edge $\partial P'/\partial n = 0$ so the corresponding a_I will be zero and the pressure will be obtained from a zero gradient extrapolation. The linear system is iteratively solved using a Gauss-Seidel relaxation procedure up to a reasonable reduction of the initial error.

Once P' is available, the pressure, the velocity components and the normal velocity are corrected.

$$P_P = P_P^* + r_P P', \quad W_P = W_P^* - B_P \left(\frac{\partial P'}{\partial z}\right)_P,$$
$$U_P = U_P^* - B_P \left(\frac{\partial P'}{\partial x}\right)_P, \quad V_{ni} = V_{ni}^* - \overline{B}_i \frac{P'_I - P'_P}{d_{PI}} \quad (21)$$

The iterative algorithm proceeds with a new solution of the momentum equations. A good convergence index of the iterative procedure is the cell mass flow balance that appears as the source term of the pressure correction equation $\Sigma_{i=a,b,c} \dot{m}_i^*$ and governs the order of magnitude of all corrections.

Finally, one should mention that a good initial guess for the pressure field can be made from the solution of Reynolds equation. High flow regimes ($\text{Re} > 10^3 \ldots 2 \cdot 10^3$) provoke a turbulent flow and one may argue [18] that a better definition of the reduced Reynolds number is

$$\text{Re}^* = \frac{\rho V H}{\mu} \frac{H}{L} \frac{12}{k_{x,z}} \quad (22)$$

which gives a lower value than (1) because $k_{z,x} > 12$ but, nevertheless, operating conditions are beyond the limit of $\text{Re}^* = 1$. Being of elliptic type, Reynolds equation can be cast in a form similar to the pressure correction equation for which the solution framework (grid topology, interpolations, resistance coefficients, linear solver, etc.) is available.

Validations

The first validations concern one dimensional pads with linear variation of the film thickness. It is only for these simplified cases that bulk flow equations have analytic solutions [2]. Figure 3 and Fig. 4 present the results obtained for a ratio $H_{\text{inlet}}/H_{\text{exit}} = 2$ and a flow regime corresponding to $\text{Re}^* = 1$. The one dimensional pad was modeled as an elongated rectangle (Fig. 2(*a*)). Pressure boundary conditions were considered on the short edges (with no concentrated inertia effects, $1 + \xi_{\text{inlet}} = 1 - \xi_{\text{exit}} = 0$) and symmetry boundary conditions on the long ones. Both short edges were divided in two segments and both long edges in 8 segments. In order to have triangular grids of good quality all segments dividing the boundary have the same length [19]. Grid refinement was made by increasing the length of the elongated rectangle and adding discretisation segments (16, 32, etc.), while the short edge of the rectangle remained unchanged. Pressures presented in Figs. 3 and 4 are considered along the midsection parallel to the long edge of the rectangle. Due to symmetry boundary conditions, pressures in the transversal direction are constant.

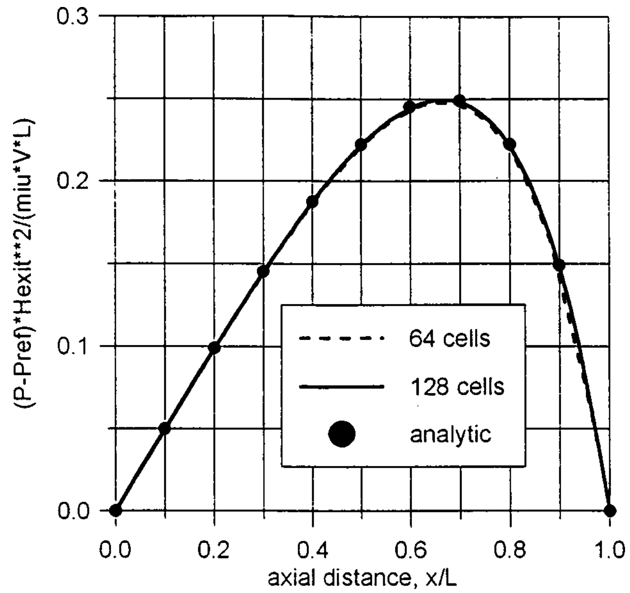

Fig. 3 Pressure distribution in a shear driven one-dimensional pad

Figure 3 presents a shear driven flow for which Re* was calculated with the relative surface velocity and the exit film thickness. The inlet and the exist pressures were the same and equal to a reference value. The analytic solution of the problem can be expressed as

$$\frac{[P(\overline{x}) - P_{\text{ref}}]H_{\text{exit}}^2}{\mu V L} = 6 \frac{\overline{H}_{\text{inlet}} - 1}{\overline{H}_{\text{inlet}} + 1} \frac{\overline{x} - \overline{x}^2}{[\overline{H}_{\text{inlet}} - (\overline{H}_{\text{inlet}} - 1)\overline{x}]^2},$$
$$\overline{x} = x/L, \quad \overline{H} = H/H_{\text{exit}} \quad (23)$$

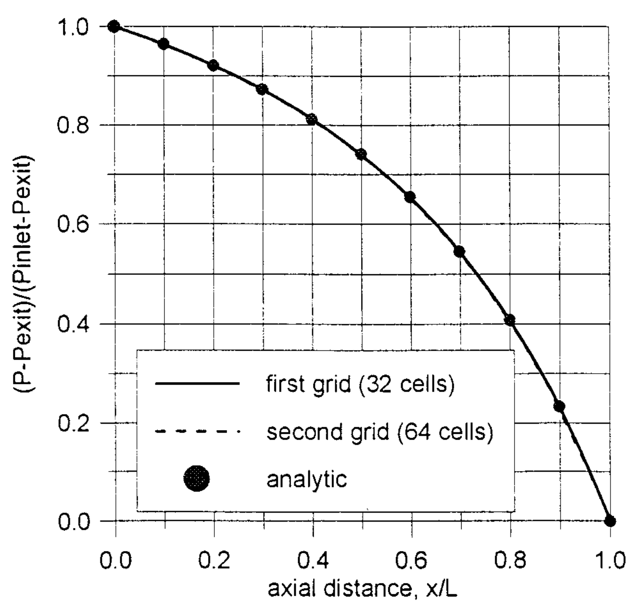

Fig. 4 Pressure distribution in a pressure driven one-dimensional pad

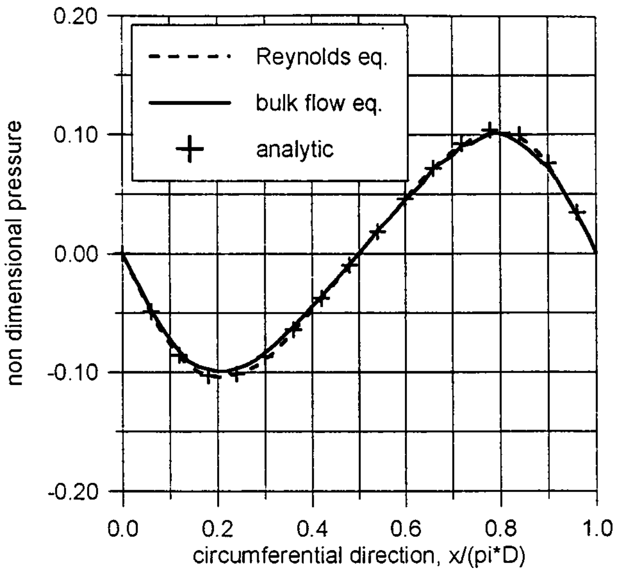

Fig. 5 Pressure variation in the midsection of a short bearing

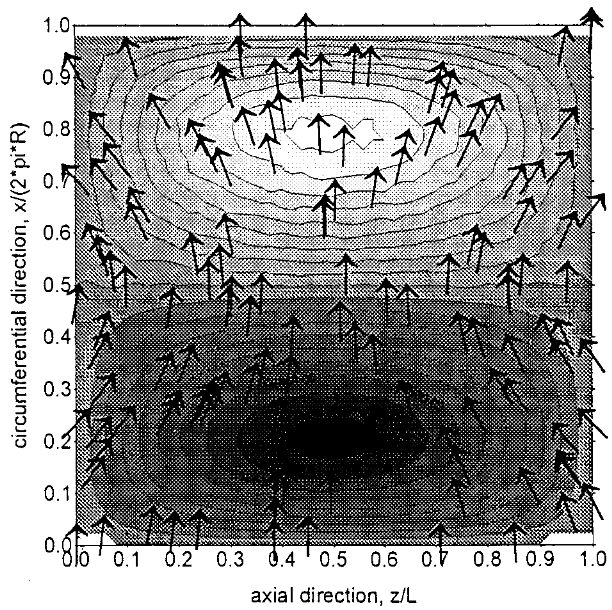

Fig. 6 Superposed pressure field (light colors—high pressure zones, dark colors—low pressure zones) and unscaled velocity vectors in a short bearing

Figure 4 presents a pressure driven flow. The reduced Reynolds number was calculated with the mass flow rate. The analytic solution used for comparison was

$$\frac{P-P_{\text{exit}}}{P_{\text{inlet}}-P_{\text{exit}}}=\frac{\overline{H}^2_{\text{inlet}}}{\overline{H}^2}\,\frac{\overline{H}^2-1}{\overline{H}^2_{\text{inlet}}-1} \tag{24}$$

The continuous (first grid) and the dashed (second grid) curves on Fig. 3 and Fig. 4 are superposed thus proving grid independent results. They both show a close agreement with the corresponding analytic solution.

A second example is the ''short bearing'' solution. This calculation is not intended to be a proper validation case but one intends to investigate the limit of the bulk flow equations and the proper behavior of pressure boundary conditions. There is no upper validity limit (in terms of Re*) for the employment of the bulk flow equations but, due to the fact that Re* appears as the coefficient of convective inertia terms (the only ones containing derivatives), an inferior limit should exist. Following this idea, the ''short bearing'' calculation ($L/D=0.25$) was made for $\text{Re}^*=0.1$ and $\varepsilon=0.1$. Results are presented on Figs. 5 and 6. Low underrelaxation coefficients used for convergence, $r_V=r_P=0.1$, proved that the lower validity limit of the bulk flow equations was approached. The grid corresponding to the developed bearing was of the type presented in Fig. 2(*b*). Periodicity boundary conditions were imposed on the short edges of the rectangles and constant pressure ones on the long edges (with no concentrated inertia effects). Pressure variation in the midsection of the bearing is presented in Fig. 5. Superposed on the same figure is the solution obtained solving Reynolds equation on the same triangular grid as well as the analytic solution taken from [20]. All solutions are in good agreement. Figure 6 presents the velocity vectors superposed on the contours of the pressure field. As cavitation wasn't taken into account, the bearing presents a pressure zone and a suction zone. Consequently, pressure boundaries will behave as in the case of a gas (compressible) bearing: the fluid will enter the bearing in the neighborhood of the suction zone and will be ejected when approaching the pressure one. In terms of numerical modeling it means that control volume edges carrying pressure boundary conditions must be able to change from inlet to exit behavior in a continuous manner. The absence of discontinuities in the velocity vectors distribution close to pressure boundaries shows that the circumferential velocity is properly convected in and out of the bearing and proves the correct behavior of the numerical boundary conditions.

Figures 7 and 8 present results obtained for turbulent annular seals. The employed meshes were similar to the grid in Fig. 2(*b*) and boundary conditions were of the same type with those used for the short bearing.

The first seal is a test case taken from the work of Amoser [21]. The geometric and operating characteristic are $R=140.2$ mm, $L=110$ mm, $H=1.8$ mm (centered), $\omega=104.72$ rad/s, $P^0_{\text{inlet}}=2.38$ bar, $\xi_{\text{inlet}}=0.59$, $V_{t\ \text{inlet}}/\omega R=0.35$ (prerotation), $P^0_{\text{exit}}=1$ bar and no exit pressure recovery, $\rho=998.5$ kg/m3, $\mu=10^{-3}$ Pa·s. The seal operates at 40 percent eccentricity. A grid independence study is carried out in Table 2. The differences between calculated results and Amoser's measurements are only apparent. They are explained by the axial distributed forces in Fig.

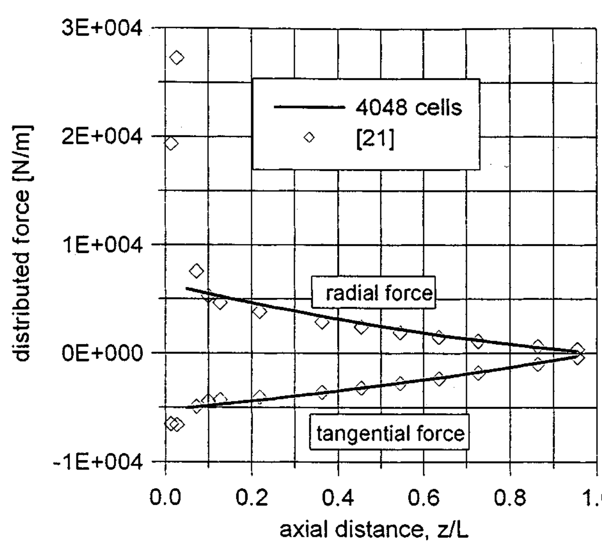

Fig. 7 Radial and tangential force components in an eccentric annular seal

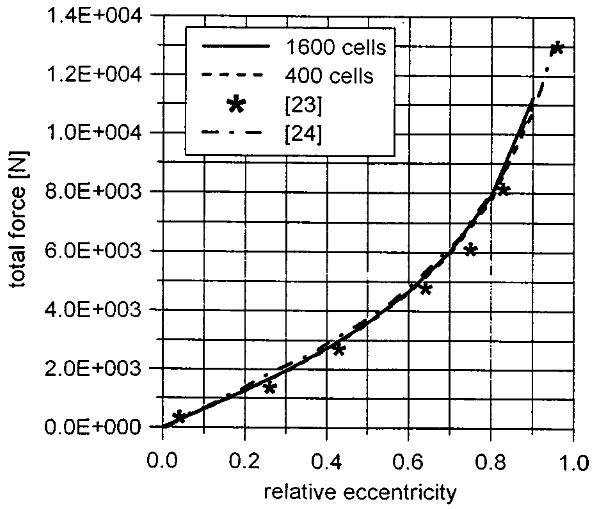

Fig. 8 Total force in a straight annular seal

Table 2 Grid independence study of an annular seal

	Amoser (1995)	254 cells	1024 cells	4048 cells	16166 cells
Radial force [N]	380	298	302	303	303
Tangential force [N]	-318	-303	-309	-312	-313

7 and are due to the inlet effects that cannot be modeled by the thin film approach. The problem was extensively argued elsewhere [22].

The second test case is taken from some of Kanki and Kawakami's [23] experimental results. The geometric and operating conditions were taken from the work of San Andrès [24]: $R=100$ mm, $L=200$ mm, $H=0.5$ mm (centered), $\omega=209.44$ rad/s, $P^0_{\text{inlet}}=14.7$ bar, $\xi_{\text{inlet}}=0.3$, $V_{t\ \text{inlet}}/\omega R=0.2$ (prerotation), $P^0_{\text{exit}}=4.9$ bar and no exit pressure recovery, $\rho=10^3$ kg/m^3, $\mu=0.9\cdot 10^{-3}$ Pa·s. The calculated mass flow rate for $\varepsilon=0$ was 4.79 kg/s showing a small discrepancy with the 4.61 kg/s measured value. The variation of the total force with eccentricity is presented in Figure 8. It shows a good agreement with measurements and with San Andrès' theoretical results obtained on a rectangular staggered grid.

Conclusions

The present work introduced a numerical method for the solution of Lubrication's bulk flow equations. A collocated version of the SIMPLE algorithm was presented and the central point of the approach was the unstructured triangular grid. The advantage of such grids is their flexibility to deal with irregular domains. In this context, the present work is the first step towards the analysis of bearings with arbitrarily shaped pockets and grooves that cannot be tackled with rectangular control volumes.

The work is focused on the description of the discretized incompressible bulk flow equations and of the solution algorithm. Validations are made by comparison with analytic results (one dimensional pad, short journal bearing) or experimental ones (turbulent annular seals) and show its accuracy.

Nomenclature

$a_{A,B,C,S}$ = terms of the linear system
B = pressure gradient coefficient
d = distance (m)
f = friction coefficient
H = film thickness (m)
$k_{x,z}=(f_R\,\mathrm{Re}_R+f_S\,\mathrm{Re}_S)/2$ = resistance coefficients
L = characteristic length (m)
$\dot{m}$ = mass flow rate (kg/s)
$\vec{n}$ = edge normal direction
P = pressure (Pa)
R = rotor (journal) radius (m)
r = underrelaxation coefficient
Re = Reynolds number
S = source term
U = circumferential velocity (m/s)
V = resultant velocity (m/s)
$V_n=\vec{V}\cdot\vec{n}$ = edge normal velocity (m/s)
W = axial velocity (m/s)
$x=R\theta$ = circumferential direction
z = axial direction
γ = edge length (m)
$\Gamma=\bigcup_i \gamma_i$ = control volume boundary
ε = relative eccentricity
ξ = concentrated inertia coefficient
$\vec{\zeta}$ = direction between centers of two adjacent cells
θ = angular coordinate (rad)
μ = dynamic viscosity (Pa·s)
ρ = density (kg/m^3)
τ = shear stress (N/m^2)
ω = rotation speed (rad/s)
ϑ = control volume surface (m^2)
Ξ = generic field variable

Indices

i, I = indices associated with edges (a, b, c) and adjacent volumes (A, B, C)
P = current control volume
R, S = rotor (journal), stator (bearing)
n, t = normal and tangential direction

Exponents

1OP = first order precision
HOP = higher order precision
0 = stagnation values
"*" = prediction values
"′" = correction values

References

[1] Constantinescu, V. N., 1995, *Laminar Viscous Flow*, Springer-Verlag, New York, NY.
[2] Milne, A. A., 1959, "On the Effect of Lubricant Inertia in the Theory of Hydrodynamic Lubrication," ASME J. Basic Eng., **81**, pp. 239–244.
[3] Kahlert, N., 1948, "Der Einfluss der Trägheitskräfte in der hydrodynamischer Schmiermitteltheorie," Ing. Arch., **16**, pp. 321–342.
[4] Slezkin, N. A., and Targ, S. M., 1946, "On the Solution of Reynolds Equation," (in Russian), Dokl. Akad. Nauk SSSR, **54**, pp. 25–208.
[5] Childs, D. W., 1993, *Turbomachinery Rotordynamics: Phenomena, Modeling and Analysis*, Wiley Interscience, New York.
[6] Launder, B. E., and Leschziner, M., 1978, "Flow in Finite-Width, Thrust Bearings Including Inertial Effects," ASME J. Lubr. Technol., **100**, pp. 330–338.
[7] Patankar, S. V., 1980, *Numerical Heat Transfer and Fluid Flow*, McGraw-Hill, New York.
[8] Donea, J., 1991, "Generalized Galerkin Methods for Convection Dominated Transport Phenomena," Appl. Mech. Rev. **44**, pp. 205–214.
[9] Glowinski, R., and Pironneau, O., 1992, "Finite Element Methods for Navier-Stokes Equations," Annu. Rev. Fluid Mech., **24**, pp. 167–204.
[10] Rhie, C. M., and Chow, W. L., 1983, "A Numerical Study of the Turbulent Flow Past an Isolated Airfoil with Trailing Edge Separation," AIAA J., **21**, pp. 1525–1532.

[11] Peric, M., 1985, ''A Finite Volume Method for the Prediction of Three-Dimensional Fluid Flow in Complex Ducts,'' Ph.D. thesis, University of London.
[12] Mathur, S. R., and Murthy, J. Y., 1997, ''A Pressure-Based Method for Unstructured Meshes,'' Numer. Heat Transfer, Part B, **31**, pp. 195–215.
[13] Lai, Y. G., 1997, ''An Unstructured Grid Method for A Pressure-Based Flow and Heat Transfer Solver,'' Numer. Heat Transfer, Part B, **32**, pp. 267–281.
[14] Hirs, G., 1973, ''A Bulk Flow Theory for Turbulence in Lubricant Films,'' ASME J. Lubr. Technol., **95**, April, pp. 137–146.
[15] Ferziger, J. H., and Peric, M., 1996, *Computational Methods for Fluid Dynamics*, Springer-Verlag.
[16] Venkatakrishnan, V., 1995, ''Convergence to Steady State Solutions of the Euler Equations on Unstructured Grids with Limiters,'' J. Comput. Phys. **118**, pp. 120–130.
[17] Majumdar, S., 1988, ''Role of Underrelaxation on Momentum Interpolation for Calculation of Flow With Nonstaggered Grids,'' Numer. Heat Transfer, **13**, pp. 125–132.
[18] Constantinescu, V. N., et al., 1985, *Sliding Bearings*, Allerton Press.
[19] George, P. L., 1991, *Automatic Mesh Generation. Application to Finite Element Methods*, Wiley, New York.
[20] Frêne, J., Nicolas, D., Degueurce, B., Berthe, D., and Godet, M., 1990, *Lubrification Hydrodynamique. Paliers et butées*, Editions Eyrolles.
[21] Amoser, M., 1995, ''Strömungsfelder und Radialkräfte in Labyrinthdichtungen hydraulischer Strömungsmascinen,'' Dissertation ETH Zurich Nr. 11150.
[22] Arghir, M., and Frêne, J., 1999, ''A Quasi-Two-Dimensional Method for The Rotordynamic Analysis of Centered Labyrinth Liquid Seals'' ASME J. Eng. Gas Turbines Power, **121**, pp. 144–152.
[23] Kanki, H., and Kawakami, T., 1984, ''Experimental Study on the Dynamic Characteristics of Pump Annular Seals,'' *Proceedings of the Institution of Mechanical Engineers*, Paper C297/84, London, United Kingdom, pp. 159–166.
[24] San Andrès, L. A., 1991, ''Analysis of Variable Fluid Properties, Turbulent Annular Seals,'' ASME J. Tribol., **113**, pp. 694–702.